AEDC-TR-66-43

RELAXATION TO THE STEADY STATE IN A CONDUCTING NONEQUILIBRIUM PLASMA STREAM

Bill P. Curry

ARO, Inc.

April 1966

PROPULSION WIND TUNNEL FACILITY
ARNOLD ENGINEERING DEVELOPMENT CENTER
AIR FORCE SYSTEMS COMMAND
ARNOLD AIR FORCE STATION, TENNESSEE

NOTICES

When U. S. Government drawings specifications, or other data are used for any purpose other than a definitely related Government procurement operation, the Government thereby incurs no responsibility nor any obligation whatsoever, and the fact that the Government may have formulated, furnished, or in any way supplied the said drawings, specifications, or other data, is not to be regarded by implication or otherwise, or in any manner licensing the holder or any other person or corporation, or conveying any rights or permission to manufacture, use, or sell any patented invention that may in any way be related thereto.

Qualified users may obtain copies of this report from the Defense Documentation Center.

References to named commercial products in this report are not to be considered in any sense as an endorsement of the product by the United States Air Force or the Government.

RELAXATION TO THE STEADY STATE IN A CONDUCTING NONEQUILIBRIUM PLASMA STREAM

Bill P. Curry
ARO, Inc.

AF - AEDC
Arnold AFS Tenn

FOREWORD

The work reported herein was sponsored by Headquarters, Arnold Engineering Development Center (AEDC), Air Force Systems Command (AFSC) under Program Element 65402234.

The results of research presented were obtained by ARO, Inc. (a subsidiary of Sverdrup and Parcel, Inc.), contract operator of AEDC, AFSC, Arnold Air Force Station, Tennessee, under Contract AF40(600)-1200. The research was conducted under ARO Project No. PT3000, and the manuscript was submitted for publication on February 8, 1966.

This technical report has been reviewed and is approved.

Robert H. LaBounty
1/Lt, USAF
Technology Division,
Experimental Branch
DCS/Plans and Technology

Donald D. Carlson
Colonel, USAF
DCS/Plans and Technology

ABSTRACT

The relaxation of a seeded plasma subjected to a constant electric field is considered within the formalism of the two-temperature theory. Numerical solutions are obtained for streamwise conductivity profiles in both argon and nitrogen plasmas seeded with potassium. Reaction rates used here are analytical formulae based on the Byron model for collision-induced recombination. Extensive analysis of the computed results and comparison with Zukoski's experiments in argon establish the validity of the basic treatment and suggest the existence of energy losses resulting from excitation of argon transitions originating at the first excited state, in addition to the usual elastic collision and potassium excitation energy losses. Refined agreement between theory and experiment requires consideration of corrections to the species-averaged momentum-transfer cross section, after the manner of Frost; however, present theories are shown to overestimate this correction for argon. Details of the Byron model are validated by comparison of theoretical and experimental time-resolved potassium emission lines. Possible nonequilibrium effects in nitrogen are investigated with various assumed molecular excitation losses. Relaxation times for both types of plasmas are correlated by use of Zukoski's characteristic time parameter.

CONTENTS

ILLUSTRATIONS

NOMENCLATURE

a	Curve fit parameter in Eq. (11)
b	Curve fit parameter in Eq. (9)
E	Electric field strength, $\frac{\text{volts}}{\text{cm}}$
F	Collision integral in Eq. (5)
$\mathfrak{z}$	Ratio of electron-collision-induced ionization from multiple excitation collisions to direct ionization from ground state
f_e^0	Isotropic electron-velocity distribution
f_e^1	Anisotropic electron-velocity distribution
g	Degeneracy
h	Planck's constant
I	Radiation line intensity
j_e	Current density, $\frac{\text{amp}}{\text{cm}^2}$
k	Boltzmann's constant
ℓ_M	Maximum orbital quantum number in interval between ground-state and state one principal quantum number above it

M	Heavy particle mass
m_e	Electron mass
N_o	Effective ground-state quantum number (true quantum number diminished by quantum defect)
n_i	Species number density
n^*	Excited-state number density
p	Pressure
Q_i	Momentum-transfer collision cross section for "ith" species
$\overline{Q}$	Species-averaged cross section
$\overline{Q}_i$	Velocity-averaged "ith" species cross section
q_e	Electronic charge
S	Energy-loss ratio in Eq. (20)
T	Gas temperature
T_e	Electron temperature
U	Stream velocity
W	Power density associated with initial extrathermal ionization
x	Stream coordinate
$\delta = \frac{\Sigma_i n_i Q_{io} \delta_i}{\Sigma n_i \overline{Q}_i}$	Species-averaged energy-momentum-loss parameter
δ_i	Energy-momentum-loss parameter for "ith" species
ϵ	Potassium ionization potential
ϵ_c	Critical energy level discussed in Section 2.2
ϵ_{ex}	Excitation potential for electron-collision-induced transition producing emission of radiation
ϵ_o	Permittivity of vacuum
ϵ^*	Excited-state energy level
ν_{ex}	Frequency of electron collisions exciting transitions through interval ϵ_{ex}
$\xi = \frac{m_e v_e^2}{2kT_e}$	Dimensionless electron energy
ρ_e	Electron-mass density

σ	Conductivity, $\frac{\text{mho}}{\text{cm}}$
Φ	Saha equilibrium constant for potassium ionization

SUBSCRIPTS

A	Argon
e	Electron
i	Species index
K	Potassium
N	Nitrogen
o	Denotes reference value

SECTION I
INTRODUCTION

The relaxation of an alkali-seeded plasma perturbed by a constant applied electric field is of importance in studies of nonequilibrium conducting plasma flows for two basic reasons: (1) for understanding the flow and predicting the performance of magnetohydrodynamic (MHD) energy-conversion devices and (2) as a test of the adequacy of the two-temperature nonequilibrium plasma theory developed by various authors and summarized in Ref. 1.

In the first case, we note that there are conditions under which a substantial portion of the MHD channel length is required for a perturbed plasma to reach a steady state. These conditions not only require consideration in the design of MHD channels but also influence possible electrothermal instabilities (discussed in Ref. 1). Even when equilibrium conditions prevail in the plasma core, nonequilibrium phenomena dominate the electrode-boundary-layer region. In all these MHD flow problems relaxation effects are of considerable interest.

In addition to its significance in MHD channel problems, the relaxation problem provides an important test of the two-temperature theory of nonequilibrium conduction, including the mechanisms of electron-energy loss. Although nonequilibrium electron-fluid descriptions abound in the literature, Kerrebrock's (Ref. 1) assumption of a Maxwell-Boltzmann distribution of both free and valence electrons, maintained at a higher temperature than the bulk gas temperature, reduces the description of nonequilibrium conduction to a tractable problem and provides a means of comparing the effects of various electron-collision energy-loss mechanisms with experimental conduction data. These assumptions are, generally, quite good for electron-collision-dominated plasmas. The experiments of Refs. 2 and 3 show that satisfactory agreement between experiments and theory can be obtained at steady-state conditions, provided proper account is taken of the various electron-collision effects. In the present investigation, detailed comparison of theoretical predictions with the relaxation experiments reported in Ref. 3 indicates that the two-temperature theory, modified to include ionization and recombination, is adequate for the full description of collision-dominated, relaxing, nonequilibrium plasmas.

SECTION II
BASIC MODEL

2.1 ASSUMPTIONS AND PROPERTIES OF THE ELECTRON-FLUID THEORY

The electron fluid can be adequately described for the present study by using conservation equations obtained as moments of Boltzmann's equation, for the electrons and their energy. For a plasma flowing at constant velocity with applied electric field perpendicular to the stream, neglecting anisotropic stresses and heat conduction, the streamwise electron-energy transport equation is

$$U \frac{d}{dx}\left(\frac{\rho_e U^2}{2} + 3/2\ p_e\right) = j_e\ E + n_e \frac{d}{dt}\left(\frac{m_e v_e^2}{2}\right)_{coll} \tag{1}$$

Within the restrictions stated above this equation is general, and assumptions concerning isotropic electron-velocity distribution affect only the collision-energy-loss term and the definition of electron temperature.

By use of the techniques of Ref. 4, one can show that the isotropic electron-velocity distribution is very nearly Maxwellian at a temperature higher than the gas temperature, provided electron-electron collisions outnumber collisions tending to distort the Maxwellian speed distribution and provided electron drift is much slower than electron-thermal motion. These conditions are assumed in the present study.

The collision term can now be specialized to Kerrebrock's form by use of the expansion of Ref. 4.

$$-\frac{d}{dt}\left(\frac{m_e v_e^2}{2}\right)_{coll} = 3/2\ \frac{m_e}{M}\ k\,(T_e - T)\,\bar{v}_e\ \Sigma_i\, n_i\, Q_{io}\,\delta_i + \frac{\epsilon}{n_e}\frac{dn_e}{dt} + \Sigma_{ex}\,\epsilon_{ex}\,\nu_{ex} \tag{2}$$

where

$$\delta_i = (4/3)\int_0^\infty \frac{Q_i(\xi)}{Q_{io}}\, e^{-\xi}\, \xi^2\, d\xi$$

and

$$\bar{v}_e = \sqrt{\frac{8}{\pi}\ \frac{kT_e}{m_e}}$$

In this equation, the first term represents elastic collision-energy loss, the second term is the electron-power loss associated with ionization, and the last term corresponds to inelastic collisions exciting

radiative transitions in an optically thin plasma. Here δ is the conventional energy-momentum-loss parameter - 2 for Maxwellian interactions, 8/3 for hard sphere collisions, and 3.952 for electron-ion collisions. The reference cross sections Q_{io} are Q_A at 0.4 ev for argon and $\overline{Q}_{ei}$ for electron-ion interactions.

The electron-fluid description is completed by the electron-conservation equation:

$$\frac{dn_e}{dt} = U \frac{dn_e}{dx} = \Im\, n_e \bar{v}_e\, \pi \left(\frac{q_e^2}{4\pi\epsilon_0 \epsilon}\right)^2 e^{-\frac{\epsilon}{kT_e}} \left[n_K - n_e\left(1 + \frac{n_e}{\Phi(T_e)}\right)\right] \tag{3}$$

where

$$\Phi(T_e) = \left(2\pi \frac{m_e kT_e}{h^2}\right)^{3/2} e^{-\frac{\epsilon}{kT_e}}$$

In this equation $\Im$ is the ionization enhancement factor representing the effect of multiple excitation collisions as opposed to "one shot" ionization collisions. It will be discussed in the next section.

2.2 ELECTRON-COLLISION-DOMINATED IONIZATION AND RECOMBINATION

A detailed discussion of ionization and recombination of hydrogen and of alkali atoms is presented in Ref. 5. Analytical formulae for the reaction rate coefficients are obtained by using Byron's assumptions (Refs. 6 and 7) along with an approximate quantum mechanical description of the atomic structure. The results for alkali atoms agree with numerical computations presented in Refs. 7, 8, and 9. Figure 1 illustrates the basic properties of the ionization model used in Ref. 5 and in the present study.

In this model all states located at or above some atomic energy level (referred to as the critical level) are in Saha equilibrium with the free electrons; i.e., their population densities are governed by the free electrons through Saha's equation. States at or below one principal quantum number below the critical state are in Boltzmann equilibrium with the ground state. The rate of ionization or recombination is equal to the net rate of crossing the critical interval, $\Delta\epsilon$, defined by the critical state and the state one principal quantum number below it.

The critical energy level is located by minimizing the reaction rates with respect to critical quantum number. This is done numerically in Refs. 7, 8, and 9 and is done analytically in Ref. 5 by using approximate expressions for the average degeneracy of states within

the critical interval, as a function of critical quantum number. The resulting analytical values of the critical energy level are in good agreement with Byron's numerical values and can be fairly well approximated at moderate electron temperatures by $\epsilon - \epsilon_c = 5k\,T_e$, where ϵ_c is the critical energy level. The critical interval is related to the critical energy level by

$$\frac{\Delta\epsilon}{kT_e} = 2\theta\,\zeta^3\,(1 + 3/2\,\theta\zeta) \tag{4}$$

where

$$\theta^2 = \frac{kT_e}{N_o^2\,\epsilon}$$

and

$$\zeta^2 = \frac{\epsilon - \epsilon_c}{kT_e}$$

The ionization enhancement factor for alkali atoms is derived in Ref. 5 in terms of these parameters:

$$\Im = \frac{1}{8}\,\frac{(1 - 5/2\,\theta\zeta)}{(N_o\,\theta^2\zeta^2)^4}\left[\frac{1}{a} - \theta\zeta\left(1 + \frac{1}{a}\right)\right]e^{\zeta^2}\,F\left(\frac{\Delta\epsilon}{kT_e}\right) \tag{5}$$

where

$$a = \frac{1 + N_o}{1 + \ell_M}$$

and

$$F\left(\frac{\Delta\epsilon}{kT_e}\right) = 0.8\left(\frac{\Delta\epsilon}{kT_e}\right)e^{\left(\frac{\Delta\epsilon}{kT_e}\right)}\int_{\frac{\Delta\epsilon}{kT_e}}^{\infty} e^{-u}\,\frac{du}{u}$$

An analogous formula for hydrogen is given in Ref. 5. Typical values of the atomic structure parameters in Eq. (5) are:

$N_O = 1.85$ and $\ell_M = 1$ for potassium

$N_O = 1.93$ and $\ell_M = 2$ for cesium

As Byron has previously demonstrated (Refs. 6 and 7), the critical energy level lowers with increasing electron temperature. In the formalism of Ref. 5, the lowest possible critical state is the state one principal quantum number above ground state; therefore, at high electron temperatures Eq. (4) must be replaced by

$$\Im_{limit} = \left(\frac{\epsilon}{\epsilon_i}\right)^2 e^{\frac{\epsilon - \epsilon_i}{kT_e}}\,F\left(\frac{\epsilon_i}{kT_e}\right)G \tag{6}$$

At this limit G is taken to be either one or the ratio of the average degeneracy for all substates in the lowest one-quantum interval to that of the ground state. Two limiting curves are generated in this fashion.

In Fig. 2, the computed three body recombination coefficients from Ref. 5 are compared with other theories and experiments of Refs. 9 and 10. Equation (5) underestimates the approach to the limit for potassium for reasons discussed in Ref. 5; however, the discrepancy is still well within experimental scatter. Equation (5) will be used here with values of ζ from Ref. 5 for all temperatures below those for which Eq. (6) is applicable.

In view of the agreement between theory and experiment shown in Fig. 2, it is not the intent of this report to verify the reaction rates computed from the Byron model. Instead, some of the assumptions of the model will be examined critically by comparing experimental and theoretical details of the excited-state relaxation in Section IV.

2.3 FINAL RELAXATION EQUATIONS

Although Eqs. (1), (2), (3), and (5) or (6) taken together with appropriate boundary conditions form a determinate set of relaxation equations, some further simplifications can be introduced into the present problem. The transport terms on the left side of Eq. (1) are orders of magnitude smaller than the terms on the right side of Eq. (1) except during an initial transient stated in Ref. 3 to be about 3×10^{-6} sec; these terms will be neglected here. Physically, this means that all energy put into the plasma by the electric field is dissipated by collisions. The electron temperature is determined by balancing energy input against dissipation. Additionally, inelastic collisions between electrons and seed atoms will be neglected because the findings of Ref. 3 indicate these energy losses to be unimportant above current densities of about $4 \frac{\text{amp}}{\text{cm}^2}$. Inelastic collisions between electrons and argon atoms will be absorbed into an effective energy-loss collision cross section in Eq. (2). Equations (1) and (2) are now combined and written as

$$\frac{q_e^2}{p} E^2 = \frac{m_e}{kT} \bar{\nu}_e \bar{Q} \left[\frac{\epsilon}{n_e} U \frac{dn_e}{dx} + \frac{3}{2} \frac{m_e}{M} k (T_e - T) \Sigma_i n_i \delta_i Q_{io} \bar{\nu}_e \right] \quad (7)$$

where

$$\bar{Q} = \Sigma_i \frac{n_i kT}{p} \bar{Q}_i$$

The average momentum-transfer cross section for the "ith" species is

$$\bar{Q}_i = \frac{3\pi}{S} \Big/ \int_0^\infty \frac{e^{-\xi} \xi}{Q_i(\xi)} \, d\xi \quad (8)$$

Frost (Ref. 11) has shown that errors are introduced by this averaging procedure. The effect of these errors will be considered in Section IV.

The relaxation is now described by simultaneous solution of Eqs. (7), (3), and (5) or (6), subject to the boundary condition that the initial electron density is some given value. In practice, the solution is obtained by finite difference integration of Eq. (3) with the electron temperature at each value of x being obtained by iteration of Eq. (7) until the specified electric field is obtained.

SECTION III
COLLISION INTEGRALS

The collision integrals appearing in Eqs. (2) and (8) are of the form of Laplace transforms of the collision cross sections. Unfortunately, they can be solved explicitly only for Maxwellian interactions, Coulomb interactions, and hard sphere collisions. In Ref. 3 these integrals were obtained numerically for each separate electron temperature. In this report the argon cross section integrals will be computed by analytic integration of curve fits to the cross sections shown as functions of electron energy in Ref. 3. Systematic variation of the curve fit parameters away from the correct elastic collision values permits simulation of inelastic collisions exciting argon radiative transitions. Potassium and nitrogen will both be treated as hard sphere gases.

The momentum-transfer integral can be calculated to sufficient accuracy by a curve fit for the argon cross section of the form

$$\frac{Q_A(\xi)}{Q_{Ao}} = \sqrt{\frac{\xi_o}{\xi}}\, e^{\left[\sqrt{\frac{\xi}{\xi_o}} - 1 + b\xi_o\left(\sqrt{\frac{\xi}{\xi_o}} - 1\right)^2\right]} \tag{9}$$

where

$$\xi_o = \frac{0.4\ \text{ev}}{kT_e}$$

and

$$Q_{Ao} = 3.82 \times 10^{-17}\ \text{cm}^2$$

The analogous cross section for electron-ion interactions is conventional:

$$Q_{e_I} = \frac{\pi}{0.582}\left(\frac{q_e^2}{2\pi\epsilon_o m_e}\right)^2 \frac{\ell n \lambda}{v_s^4}$$

where λ is the ratio of Debye length to the 90-deg deflection impact parameter.

Provided $b\xi_o > 1/2$, the integrated argon cross section becomes

$$\bar{Q}_A = \frac{3\pi}{8} \frac{Q_{Ao}}{I_Q} \tag{10}$$

where

$$I_Q = \int_o^\infty \frac{Q_{Ao}}{Q(\xi)} e^{-\xi} \xi d\xi = \frac{e^{1-b\xi_o}}{\sqrt{\xi_o}(1+\beta)^{5/2}} \left\{ \sqrt{\pi}\ e^{\beta^2} \left[1 + \text{erf}(\beta)\right] \left[3/4 + \beta^2(3+\beta^2)\right] + \beta(11/2 + 15\beta^2) \right\}$$

and

$$\beta = \frac{b\xi_o - 1/2}{\sqrt{\xi_o(1+b)}}$$

The integrated electron-ion cross section is

$$\bar{Q}_{e_i} = \frac{\sqrt{\frac{\pi}{8}}}{0.591} \left(\frac{q_e^2}{4\pi\epsilon_o kT_e} \right)^2 \ell n \lambda$$

as used in Ref. 3.

The energy-loss integral in Eq. (2) cannot be calculated from Eq. (9) because of convergence difficulty. Instead, Eq. (9) is used for $\xi \leq \xi_o$, and a parabolic curve fit is used for $\xi \geq \xi_o$.

$$\frac{Q_A(\xi)}{Q_{Ao}} = 1 + a(\xi - \xi_o)^2 \tag{11}$$

The energy-momentum parameter, δ_A, for argon now becomes

$$\delta_A = 4/3 \frac{e^{(b\xi_o - 1)}}{(1-b)^3} \left\{ \left| \frac{1/2 - b\xi_o}{1-b} \right| (5/2 + Z) + e^{(Z - Z_o)} \left[\sqrt{\left| \frac{Z_o \xi_o}{1-b} \right|} (3 + Z_o + 6Z) - 4 \left| \frac{1/2 - b\xi_o}{1-b} \right| (1 + Z_o + Z) \right] + \sqrt{\xi_o}\ e^Z (3/4 + 3Z + Z^2) \left[\sqrt{\frac{\pi}{1-b}} \left(\text{erf}(\sqrt{Z}) - \text{erf}(\sqrt{Z_o}) \right) \right] \right\} + 4/3 \left[1 + a\xi_o^2 \Gamma_{(3,\xi_o)} - 2a\xi_o \Gamma_{(4,\xi_o)} + a\Gamma_{(5,\xi_o)} \right] \tag{12}$$

where

$$Z = \frac{(1/2 - b\xi_o)^2}{(1-b)\xi_o}, \quad Z_o = \frac{(\xi_o - 1/2)^2}{(1-b)\xi_o}$$

and

$$\Gamma_{(n,\,\xi_o)} = \int_{\xi_o}^{\infty} e^{-\xi}\,\xi^{n-1}\,d\xi$$

Matching the argon Ramsauer-Townsend cross sections used in Ref. 3 yields $b\xi_o = 5.371$ and $a\xi_o^2 = 0.8752$. The collision integrals obtained from these parameters are shown in Figs. 3 and 4 for comparison with the results of numerical integration. The analytical approximations are, obviously, adequate for use in the present study. Also shown in Fig. 4 is a curve obtained from $b\xi_o = 5.371$ and $a\xi_o^2 = 4.5$. It represents additional energy loss resulting from inelastic collisions and will be discussed in Section IV.

SECTION IV
COMPARISON OF THEORETICAL RESULTS WITH ZUKOSKI'S EXPERIMENTS IN POTASSIUM-SEEDED ARGON

The conductivity and current density can be calculated from the primary relaxation solutions by use of the equations below.

$$\sigma = \frac{n_e q_e^2 kT}{m_e \bar{\nu}_e \bar{Q} p} \tag{13}$$

and

$$j_e = \sigma E \tag{14}$$

These quantities will be compared with the data reported in Ref. 3 in the following fashion: First, the steady-state conductivity will be shown as a function of current density with only elastic collisions accounted for. Second, the energy-momentum-loss parameter will be adjusted until theory and experiments agree well in the steady state, and the energy-loss curve generated by this procedure will be interpreted quantitatively as an excitation mechanism. Third, the streamwise variation of conductivity with time computed using this energy loss will be compared with the experimental relaxation profiles. Fourth, the excited-state behavior of potassium will be computed from the properties of the Byron model for ionization and recombination and correlated with time-resolved spectra reported in Ref. 3. After the adequacy of the basic treatment has been established, a summary of the relaxation process will be presented from analysis of the relaxation solutions.

As these calculations assume somewhat idealized conditions, it is well to review the theoretical restrictions and the implications of effects not taken into account before comparing theory and experiments.

1. The theory assumes the electrons instantaneously achieve equilibrium with the electric field, yielding an initial electron temperature consistent with Eq. (7) at a given initial electron density. Experimentally, however, a finite time is required for the electrons to reach this condition.

2. Excitation of the seed has been neglected because it was shown in Ref. 3 to be unimportant at current densities above $4 \frac{\text{amp}}{\text{cm}^2}$. This neglect causes some overestimation of quantities in the early relaxation region.

3. Anisotropic electron-velocity effects are assumed to be described adequately by the integral in Eq. (8). The rather drastic dependence of the electron-argon collision cross section on electron energy should narrow the anisotropic velocity distribution with respect to that used in Eq. (8).

4. A related consideration is the use of species-averaged collision frequencies within the integral used in Eq. (8) instead of averaging over species after performing the velocity integration. A rigorous consideration of these last two effects is beyond the scope of this report; however, it will be shown later in this section that present methods of dealing with these two effects are completely inadequate in the case of seeded argon. More work of both experimental and theoretical character is clearly needed.

4.1 STEADY-STATE RESULTS

Figure 5 shows that steady-state conductivities computed with only elastic collision-energy losses (corresponding to the curve marked $a\xi_o^2 = 0.8752$ in Fig. 4) agree only fairly well with quoted experimental results. The present calculations for elastic collisions are exhibited at only one seed rate $\left(\frac{n_K}{n_A} = 0.0023\right)$ because at all seed rates the results are virtually identical with similar ones taken from Ref. 3. Better agreement between theory and experiments is obtained by use of the energy-loss curve (in Fig. 4) labeled $a\xi_o^2 = 4.5$. This curve was generated by forcing the computed conductivity to agree with experimental data at one seed rate $\left(\frac{n_K}{n_A} = 0.0047\right)$. Figure 5 shows that the resulting theoretical conductivities agree well with experimental results at all seed rates. A plausible mechanism for this additional energy loss will now be considered in detail.

Since the first excited state of argon is metastable, its population density is higher than that obtained by Boltzmann equilibrium with the ground state. (Its population corresponds, roughly, to that in the arc column.) A likely electron-energy-loss mechanism, then, is excitation of higher argon states by collisional transitions originating at the metastable level. These higher states should then decay by allowed radiative transitions. The presence of metastable argon atoms also implies an additional ionization mechanism (associated with collisional de-excitation), hence a mechanism for electron-energy gain. Including both these effects, the inelastic collision energy-momentum-loss parameter for argon with metastable states follows.

$$\delta_{A_{inelastic}} = 2/3 \frac{M}{m_e Q_{Ao} k(T_e - T)} \left[0.4 \pi \left(\frac{q_e^2}{4\pi\epsilon_o} \right)^2 \frac{e^{-\left(\frac{\epsilon_{ex}}{kT_e}\right)}}{\epsilon_{ex}} \frac{n_A^*}{n_A} - \frac{\epsilon_A^*}{n_e n_A \bar{v}_e} \frac{dn_A^*}{dt} \right] \tag{15}$$

where ϵ_{ex} is the excitation potential for the transition under consideration, ϵ_A^* is the energy level of the metastable state from which the transition originates, and n_A^* is the population density of that state.

The first term in Eq. (15) represents energy loss resulting from excitation of the transitions mentioned. The second term represents energy put into the electron gas by destruction of metastable states resulting from argon-potassium ionization collisions. This term is negligible except in the early stages of the relaxation and is omitted from the relaxation solutions.

The metastable population can be estimated by equating the power density supplied by the metastables to that required to produce the extrathermal initial ionization observed in the experiments of Ref. 3. The initial conductivities obtained in the relaxation experiments of Ref. 3 are about $0.5 \frac{\text{mho}}{\text{cm}}$, contrasted with gas thermal conditions an order of magnitude lower. The electron temperature required to produce such conduction is related to the conductivity by

$$\sigma = \sqrt{\frac{\pi}{8}} \frac{q_e^2 n_e kT}{\sqrt{m_e kT_e}\, \bar{Q} p} \tag{16}$$

This corresponds to a required power density obtained from the steady-state portion of Eq. (7),

$$W = \frac{6\bar{Q}}{\sqrt{2\pi m_e kT_e}} pkT \frac{m_e}{M} \delta \frac{T_e}{T} \left(\frac{T_e}{T} - 1 \right) n_e \tag{17}$$

The power density supplied by the metastables is

$$W = \epsilon^* \frac{dn_A}{dt} = \epsilon^* n_A^* n_K Q_{KA^*} \sqrt{\frac{8}{\pi} kT \left(\frac{1}{M_A} + \frac{1}{M_K} \right)} \tag{18}$$

where Q_{KA^*} is the cross section for potassium atom-argon metastable atom collisions. It is approximately $\frac{n_A^*}{n_A} Q_K$. The use of these equations yields, for $\sigma = 0.48 \frac{\text{mho}}{\text{cm}}$ and $\frac{n_K}{n_A} = 0.0047$, $\frac{n_A^*}{n_A} = 3.3 \times 10^{-5}$ corresponding to an arc column temperature of about 10,000°K.

The only transition capable of reproducing the approximate shape of the empirical inelastic collision-energy-loss curve shown in Fig. 6 (corresponding to the difference of the two analytical curves in Fig. 4) is $1S_5 - 2P_6$ (Paschen notation). Its excitation potential is 1.623 ev (Ref. 12). When this excitation potential and the calculated metastable population density are substituted into the first term of Eq. (15), the theoretical excitation energy-loss curve shown in Fig. 6 is generated. In view of the approximate nature of the calculation, the agreement of these curves is striking. Future experimentation should certainly seek spectroscopic evidence for these excitations.

4.2 CONDUCTIVITY RELAXATION

Typical conductivity-relaxation profiles, including the effect of the argon excitation energy losses, are shown in Fig. 7 in comparison with experimental profiles from Ref. 3. The theoretical values have been set equal to the experimental values at time, t = 0, to account for the extrathermal ionization present initially in the experiments. Also shown are experimental and theoretical relaxation times corresponding to $\frac{\sigma - \sigma_{\text{initial}}}{\sigma_{\text{final}} - \sigma_{\text{initial}}} = 1 - \frac{1}{e}$. The agreement is satisfactory.

The effect on the relaxation profiles of neglecting excitation of potassium resonance radiation can now be assessed. In Ref. 5 it is shown that for cesium the ratio of radiative to collisional transitions across the lowest lying critical interval is $\frac{1.24 \times 10^{14}}{n_e}$ cm^{-3}. Since similar conditions should occur with potassium, the excitation of potassium resonance lines should be unimportant for electron densities much greater than 1.3×10^{14} cm^{-3}. The steady-state current density corresponding to this electron density is about $2 \frac{\text{amp}}{\text{cm}^2}$. Zukoski quoted a current density of about $4 \frac{\text{amp}}{\text{cm}^2}$, corresponding to electron densities of about 2×10^{14} cm^{-3}. This experimental finding lends validity to the use of times corresponding to electron densities of 1.3×10^{14} cm^{-3} as the criterion for separating regions of collisional and radiative dominance, as shown in Fig. 7. Except for very low electric fields, the relaxation profiles are, obviously, collision dominated, and the present

treatment is adequate through most of the relaxation region. The observed discrepancies between theoretical and experimental relaxation times can be entirely attributed to neglect of potassium resonance radiation.

4.3 DETAILS OF THE RELAXATION MECHANISMS

Having established the validity of the basic treatment, we can now use these solutions to shed light on the excited-state behavior of the potassium seed and other details of the relaxation process. Comparison of theoretical predictions with experimental excited-state populations obtained from time-resolved spectral measurements reported in Ref. 3 provides a sensitive test of the assumptions associated with the Byron model for ionization and recombination.

All states located at or above the critical state are described by

$$n^* = \frac{n_e^2 g^*}{g_e g_{ion}} \frac{e^{-\frac{\epsilon^*}{kT_e}}}{\Phi(T_e)} \tag{19}$$

Figure 8 compares the spectral line intensities expected from states described by Eq. (19) with experimental values from Ref. 3.

Looking first at the resonance radiation (1.61-ev experimental curve), we note that the line intensity rises sharply, reaches a plateau, and then rises more slowly to its steady-state value. In contrast, the other experimental line intensity curve rises smoothly to its steady-state value. There is fair agreement between predictions of Eq. (19) and the observed radiation for the lower curve, indicating that the critical energy level is below 3.4 ev.

The origin of the plateau in the resonance radiation corresponds closely to the attainment of the electron density (1.3×10^{14} cm^{-3}) at which collisional and radiative transitions are equal across the lowest one-quantum interval above ground state. The occurrence of this plateau and the line intensity behavior after the plateau suggests strongly that the first excited state of potassium (located at 1.61 ev) lies within the critical interval.

These considerations restrict the critical energy level at $T_e = 3100°K$ to the range from 2.61 to 3.06 ev. Reference 5 predicts $\epsilon_c = 2.67$ ev; the nearest state satisfying the assumption of a one-quantum critical interval is 5S, lying at 2.61 ev. References 5 and 8 for cesium imply that the critical state in potassium should be 5P,

corresponding to $\epsilon_c = 3.06$ ev. The Byron model is fairly well substantiated in spite of the dubious nature of some of the statistical assumptions at high electron temperature.

The dip in the electron temperature shown in Fig. 9 can be explained on the basis of competition between ionization and other collision phenomena. Let the ratio of power loss by ionization to that resulting from all other energy-loss collisions be

$$S = \frac{\epsilon}{n_e} \frac{dn_e}{dt} \Big/ 3/2 \frac{m_e}{M} \bar{v}_e k(T_e - T) \Sigma_i n_i Q_{io} \delta_i$$

Equation (7) can be rewritten as

$$E^2 = \frac{12}{\pi} \frac{m_e}{M} \frac{T_e}{T} \left(\frac{T_e}{T} - 1\right)\left(\frac{p\bar{Q}}{q_e}\right)^2 \delta(1 + S) \tag{20}$$

where

$$\delta = \frac{\Sigma_i n_i Q_{io} \delta_i}{\frac{p}{kT} \bar{Q}}$$

The most rapidly varying quantities in Eq. (20) are S and $\bar{Q}$; S decreases with time as recombination becomes important, and $\bar{Q}$ increases with time as Coulomb scattering occurs. For an ionization-dominated plasma, Eq. (20) predicts that the electron temperature should rise monotonically until the increase of $\bar{Q}$ causes it to level off. In contrast, a plasma whose ionization losses are much smaller than other losses (such as large excitation losses) should exhibit an electron-temperature decline to steady-state conditions.

The relaxation of seeded argon exhibits both these types of behavior. Figure 9 shows that the relative electron-ion collision frequency increases faster than S decreases, causing the electron temperature to decrease until the two terms balance. Beyond this time, recombination proceeds faster than the increase of electron-ion scattering, causing the electron temperature to increase to its steady-state value. This behavior is typical of plasmas in which ionization energy-loss rates are comparable to all other energy-loss rates.

4.4 UNCERTAINTIES ASSOCIATED WITH COLLISION CROSS SECTION AVERAGING PROCEDURE

The preceding discussion has shown that moderate density, alkali-seeded plasmas are well described by the two-temperature theory. In particular, the assumption of a Maxwell-Boltzmann isotropic distribution

of free electrons and bound-state electrons (above the critical state during relaxation) is adequate for the description of most collision-dependent phenomena. Unfortunately, effects dependent on the anisotropic velocity distribution can not, at present, be predicted with such certainty.

The averaged collision cross section in Eq. (7) should really be obtained from

$$\frac{kT}{p\bar{Q}} = 4/3\ \sqrt{\pi}\ \frac{m_e}{q_e E n_e}\left(\frac{2kT_e}{m_e}\right)^{5/2}\int_0^\infty \xi\, f_e^{\,1}(\xi)\, d\xi \tag{21}$$

When the approximate solution of Boltzmann's equation given in Ref. 4 is good, the ratio of anisotropic to isotropic distributions is

$$\frac{f_e^{\,1}(\xi)}{f_e^{\,0}(\xi)} = \frac{-q_e E}{kT_e}\,\frac{d\ln f_e^{\,0}(\xi)}{d\xi}\,\frac{1}{\Sigma_i n_i Q_i(\xi)} \tag{22}$$

and Eq. (21) can be rewritten as

$$\bar{Q} = \frac{3\pi}{8}\Big/\frac{p}{kT}\int_0^\infty \frac{\xi\, e^{-\xi} H(\xi)\, d\xi}{\Sigma_i n_i Q_i(\xi)} \tag{23}$$

where

$$H(\xi) = \frac{df_e^{\,0}(\xi)}{d\xi}\Big/\frac{df_e^{\,0}(\xi)}{d\xi}_{\text{Maxwellian}}$$

When scattering by any one species predominates, Eq. (23) reduces to the cross section used in Eq. (7), the form first assumed in Ref. 13 to correlate shock tube conductivity studies in unseeded argon.

For the case of H = 1, Frost (Ref. 11) has shown that when scattering by ions is comparable to neutral scattering, the conductivity is overestimated by use of the cross sections in Eq. (8) and must be ratioed down by use of a correction factor. Figure 10 shows the conductivity-correction factor (ratio of cross section given by Eqs. (8) and (23)) obtained from Eq. (23) (with H = 1) for a plasma composed of hard spheres and ions. It is slightly lower than Frost's because Frost used a different ion cross section (corresponding to a different form of the electron-electron scattering term); however, the curves are similar. Also shown are results for nitrogen obtained by using curve fits of experimental cross sections in an analytic calculation.

When Eq. (23) was evaluated numerically for partially ionized, seeded argon, the corrections were found to be more severe than those mentioned above - so severe that the conductivities shown in Fig. 5 were underestimated by almost a factor of 2. As this result is inconsistent with the good correlation of experimental data reported in

Refs. 2, 3, and 13, we are led to conclude that Eq. (23) is inadequate in argon. Two possible reasons for this inadequacy will now be explored.

First, consider the effect of electron-argon collisions on the electron-distribution function: The drastic dependence of the argon collision cross section on electron energy (resulting from the Ramsauer-Townsend effect) narrows the anisotropic velocity distribution. If the limit form $H(\xi)\, e^{-\xi} \rightarrow \delta(\xi - \xi_0)$ is used as the distribution function in both Eqs. (23) and (8), the two equations predict the same cross section, suggesting that proper results of using Eq. (23), if the velocity distribution were known correctly, should be closer to those of Eq. (8) than of Eq. (23) with the usual assumption that $H = 1$.

An alternate, but related, possibility is the following*: Occasional electron-argon collisions in a sequence of deflections resulting from electron-ion interaction may drastically change the scattered velocity distribution, affecting subsequent electron-ion collisions. Scattering under such conditions is similar to scattering resulting from a combination of Coulomb interactions and inelastic collisions. In such circumstances it is probably appropriate to perform velocity-distribution averages before averaging over species, leading to the use of Eq. (8) instead of Eq. (23). Rigorous determination of the factor H likely will require a numerical solution of the Boltzmann-Fokker-Planck equation, similar to that mentioned in Ref. 11 (for a gas composed of hard spheres, electrons, and ions). It is questionable whether such sophistication at this stage is worthwhile.

SECTION V
THEORETICAL RESULTS FOR SEEDED NITROGEN

Because of its importance in practical MHD devices, relaxing conduction in seeded nitrogen will now be studied. Lack of reliable experimental conductivity data and lack of understanding of energy-loss mechanisms will necessarily restrict the scope of this section. It is intended, however, that this study should guide future experimentation in seeded diatomic plasmas. With this purpose in mind we shall study relaxation in nitrogen at only one seed mole fraction but at various gas

*Dr. L. E. Ring, ARO, Inc., is acknowledged for this suggestion.

temperatures. Calculations will be presented using two forms of electron-energy loss associated with molecular-state excitation.

Electronic collisional excitation of diatomic molecules is not well understood. Lacking reliable excitation cross sections, we shall lump electron-neutral energy-loss collisions and arbitrarily use values of 25 and 100 for the resulting parameter

$$\delta_o = \frac{8/3\, n_K Q_K + \delta_N n_N Q_N}{\frac{p\bar{Q}}{kT}}$$

The first value corresponds to experimental nitrogen excitation losses at room temperature (Ref. 14). The second value represents a crude attempt to account for additional excitation at the high gas temperature characteristic of current MHD devices. Experimentally, $\delta_o = 100$ correlates the data of Ref. 15; however, uncertainties in the gas temperature measurement and electrode sheath and boundary-layer voltage drops obscure any conclusive analysis of the results of Ref. 15. It is probably best to view $\delta_o = 100$ as an estimated upper limit for the electron-energy loss in seeded nitrogen.

Some theoretical justification for this value can be obtained by treating electron-collisional excitation of an anharmonic oscillator. Because upper vibrational energy levels are more closely spaced than lower ones, more one-quantum excitations are possible at high gas temperature than was true in the room temperature experiments reported in Ref. 15. Assuming classical collisional-excitation probability and using energy levels for the anharmonic oscillator (Ref. 16), one can show that the inelastic portion of δ_N is approximately proportional to $\sqrt{T}$. This order of magnitude estimate predicts $\delta_o \approx 75$.

Figure 11 shows both steady-state and relaxing conductivity calculations. It is immediately apparent that experiments in an unrelaxed flow can lead to erroneously high apparent values of δ_o, if the relaxation is assumed complete. It should also be noted that experimental determination of δ_o from the curvature of the conductivity-current density curves will require very precise conductivity measurement - likely 10 percent or better. Probably, spectroscopic investigations will be required to determine δ_o accurately.

Although they are not shown here, the relaxation profiles in seeded nitrogen are very similar to those in seeded argon. In nitrogen, however, the electron temperature always stays constant or monotonically decreases with time because the large molecular excitation losses

dominate the relaxation process, as indicated in Section 4.3. This relaxation behavior is in marked contrast to that noted in argon because of the difference in collisional-energy-loss magnitudes.

The relaxation times in both nitrogen and argon are shown in Fig. 12 as functions of Zukoski's characteristic time parameter,

$$t_c = \frac{n_{e_{initial}} \epsilon}{\sigma_{initial} E^2}$$

The nonlinear curves for nitrogen indicate that relaxation in nitrogen is dominated by the large energy losses in contrast to the nearly linear curves for argon, where the relaxation is power limited. Since flow residence times in many MHD channels are of the order of 200 microseconds, the relaxation times in nitrogen at temperatures below 2500°K seem prohibitively large.

SECTION VI
CONCLUDING REMARKS

This report has considered the relaxation of a moderate density, alkali-seeded plasma subjected to a constant electric field. By correlating numerical solutions with experimental data in argon reported in Ref. 3, the adequacy of Kerrebrock's two-temperature electron-fluid theory in combination with Byron's ionization and recombination model has been established. In particular, fair agreement between theoretical and experimental conductivity is obtained when only elastic collision energy loss is considered. Allowance for inelastic collisions improves the agreement. Detailed analysis of time-resolved spectra from potassium-excited states indicates that the excited-state behavior assumed in the Byron model is approximately correct and that the critical state is correctly located.

Correlation of experimental initial conditions of Ref. 3 (extrathermal ionization) with the presence of argon metastable atoms indicates that a likely inelastic collision electron-energy-loss mechanism is the excitation of transitions originating at the metastable first excited state. Future experimentation in argon should include a spectroscopic verification of this mechanism.

The procedure for obtaining averaged momentum transfer collision cross sections is questioned. It is shown that better results are obtained in argon by use of the simple collision-frequency addition rule of Ref. 13 than by more sophisticated calculations similar to those of Ref. 11. The

latter likely fail because of inconsistencies in computing the anisotropic velocity distribution for the case in which an electron's energy changes appreciably during deflection through 90 deg.

Relaxing and steady-state conductivities in seeded nitrogen have been computed for two values of electron-energy loss caused by excitation of molecular energy levels. It is shown that very precise experiments will be required to establish conclusively these losses from conductivity measurements alone. It is suggested that spectroscopic studies be done in this area, also. Comparison of relaxation times in nitrogen and argon shows argon to be power limited, whereas the rate of relaxation in nitrogen is strongly affected by the large molecular excitation losses.

REFERENCES

1. Kerrebrock, J. L. "Nonequilibrium Ionization Due to Electron Heating: I Theory." AIAA Journal, Vol. 2, No. 6, 1964, pp. 1072-1080.

2. Kerrebrock, J. L. and Hoffmann, M. A. "Nonequilibrium Ionization Due to Electron Heating: II Experiments." AIAA Journal, Vol. 2, No. 6, 1964, pp. 1080-1087.

3. Zukoski, E. E., Cool, T. A., and Gibson, E. G. "Experiments Concerning Nonequilibrium Conductivity in a Seeded Plasma." AIAA Journal, Vol. 2, No. 8, 1964, pp. 1410-1417.

4. Allis, W. P. "Motion of Ions and Electrons." Handbuch der Physik, Vol. 21, Springer-Verlag, Berlin, 1956.

5. Curry, B. P. "Ionization and Recombination in Alkali-Seeded Collision-Dominated Plasmas." AEDC-TR-65-260, February 1966.

6. Byron, S., Stabler, P. C., and Bortz, P. I. "Electron-Ion Recombination by Collisional and Radiative Processes." Physical Review Letters, Vol. 8, No. 9, 1962, pp. 376-379.

7. Byron, S., Bortz, P. I., and Russel, G. R. "Electron Ion Reaction Rate Theory: Determination of the Properties of Non-Equilibrium Monatomic Plasmas in MHD Generators and Accelerators and in Shock Tubes." Proceedings of the Fourth Symposium on the Engineering Aspects of Magnetohydrodynamics, Berkely, California, April 1963, University of California Press, Berkely, 1963, pp. 93-101.

8. Dugan, J. V., Jr. "Three-Body Collisional Recombination of Cesium Seed Ions and Electrons in High-Density Plasmas with Argon Carrier Gas." NASA TN-D-2004, October 1964.

9. Cool, T. A. and Zukoski, E. E. "Recombination Rates and Non-Equilibrium Electrical Conductivity in Seeded Plasmas." Proceedings of the Sixth Symposium on Engineering Aspects of Magnetohydrodynamics, Pittsburgh, Pennsylvania, April 1965, pp. 122-134.

10. Wada, J. T. and Knechtli, R. C. "Measurements of Electron-Ion Recombination in a Thermal Cesium Plasma." Physical Review Letters, Vol. 10, No. 12, 1963, pp. 513-516.

11. Frost, L. S. "Conductivity of Seeded Atmospheric Pressure Plasmas." Journal of Applied Physics, Vol. 32, No. 10, 1961, pp. 2029-2036.

12. Gray, D. E., Ed. AIP Handbook. McGraw-Hill, New York, 1957.

13. Lin, S. C., Resler, E. L., and Kantrowitz, A. "Electrical Conductivity of Highly Ionized Argon Produced by Shock Waves." Journal of Applied Physics, Vol. 26, No. 1, 1955, pp. 95-109.

14. Massey, H. S. W. and Burhop, E. H. S. Electronic and Ionic Impact Phenomena, Oxford University Press, London, 1952.

15. Tempelmeyer, K. E., Windmueller, A. K., and Rittenouse, L. E. "Development of a Steady-Flow JxB Accelerator for Wind Tunnel Application." AEDC-TDR-64-261 (AD452942), December 1964.

16. Hertzberg, G. Molecular Spectra and Molecular Structure, I. Spectra of Diatomic Molecules. Van Nostrand, New York, 1950.

17. Hinnov, E. and Hirschberg, J. G. "Electron-Ion Recombination in Dense Plasmas." Physical Revue, Vol. 125, No. 3, 1962, pp. 795-801.

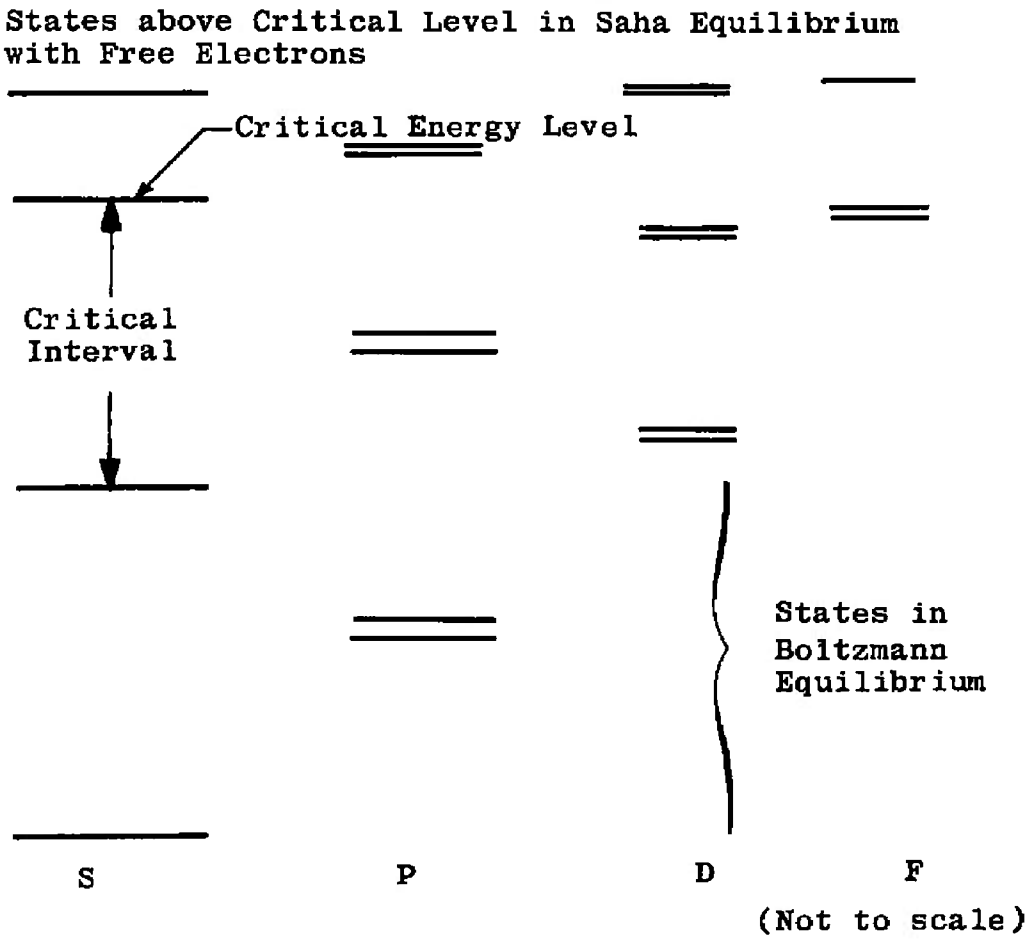

Fig. 1 Model of Alkali Atomic Structure Used in Reaction Rate Calculations

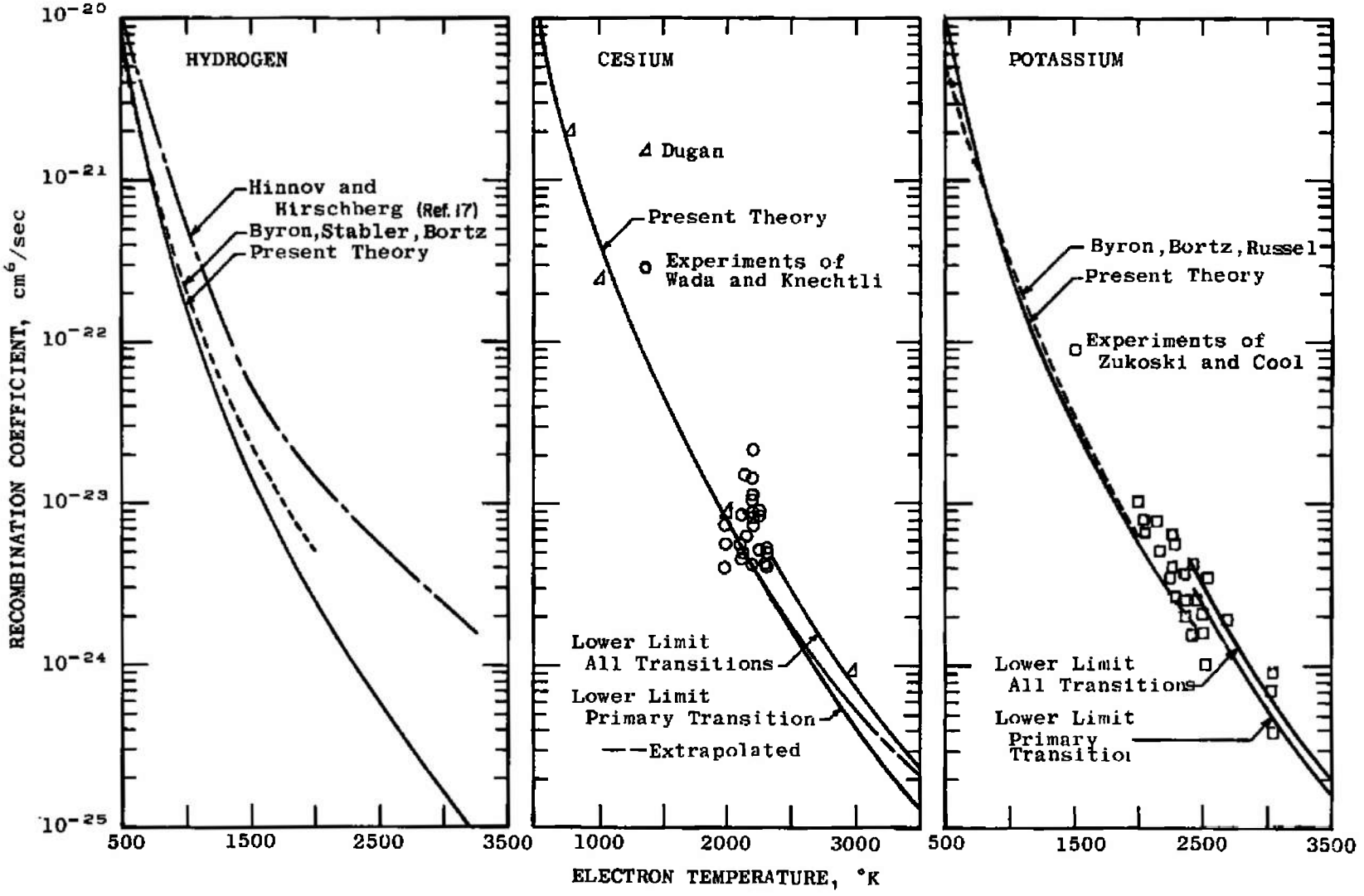

Fig. 2 Collisional Recombination Rates

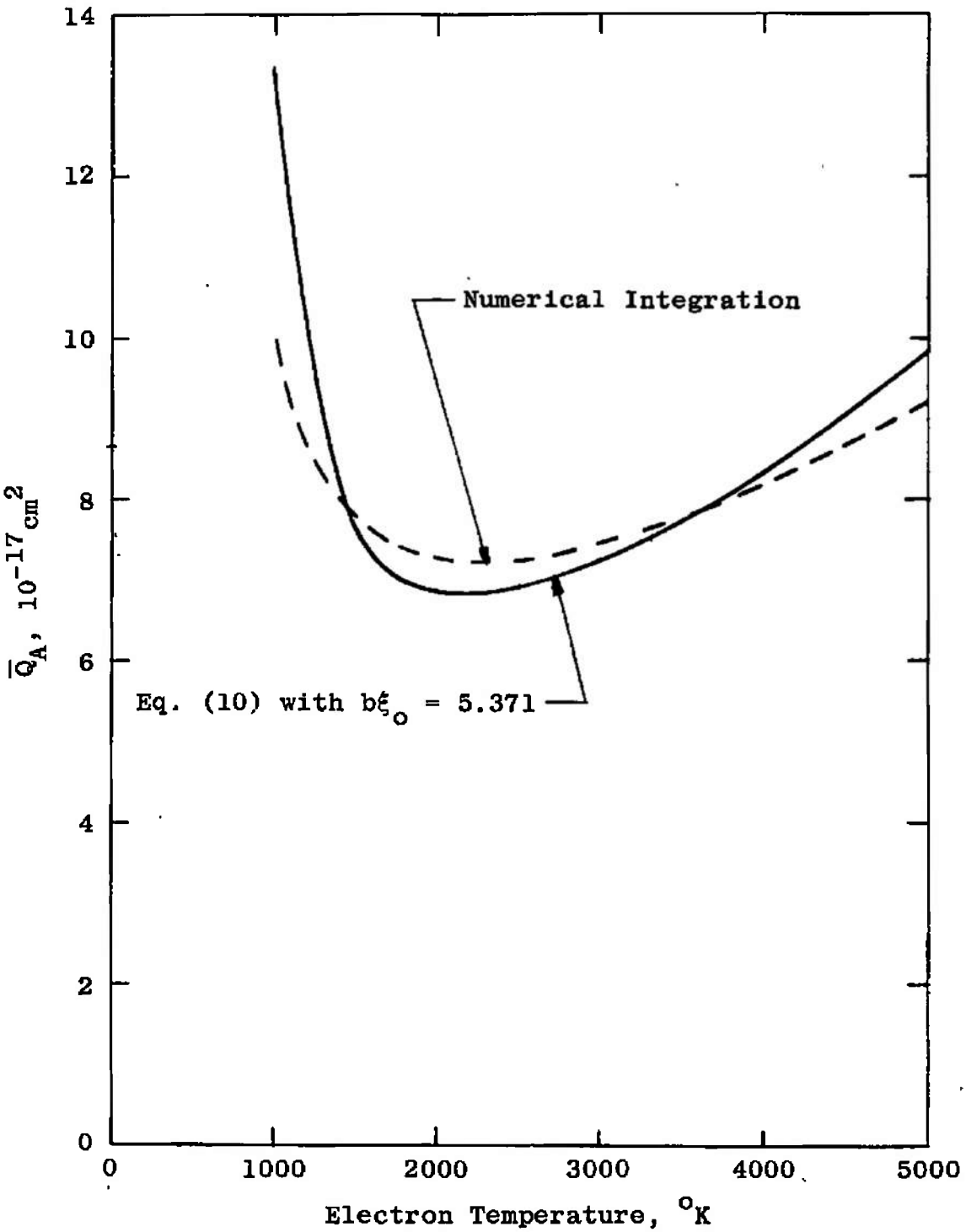

Fig. 3 Averaged Electron-Argon Elastic Collision Cross Section

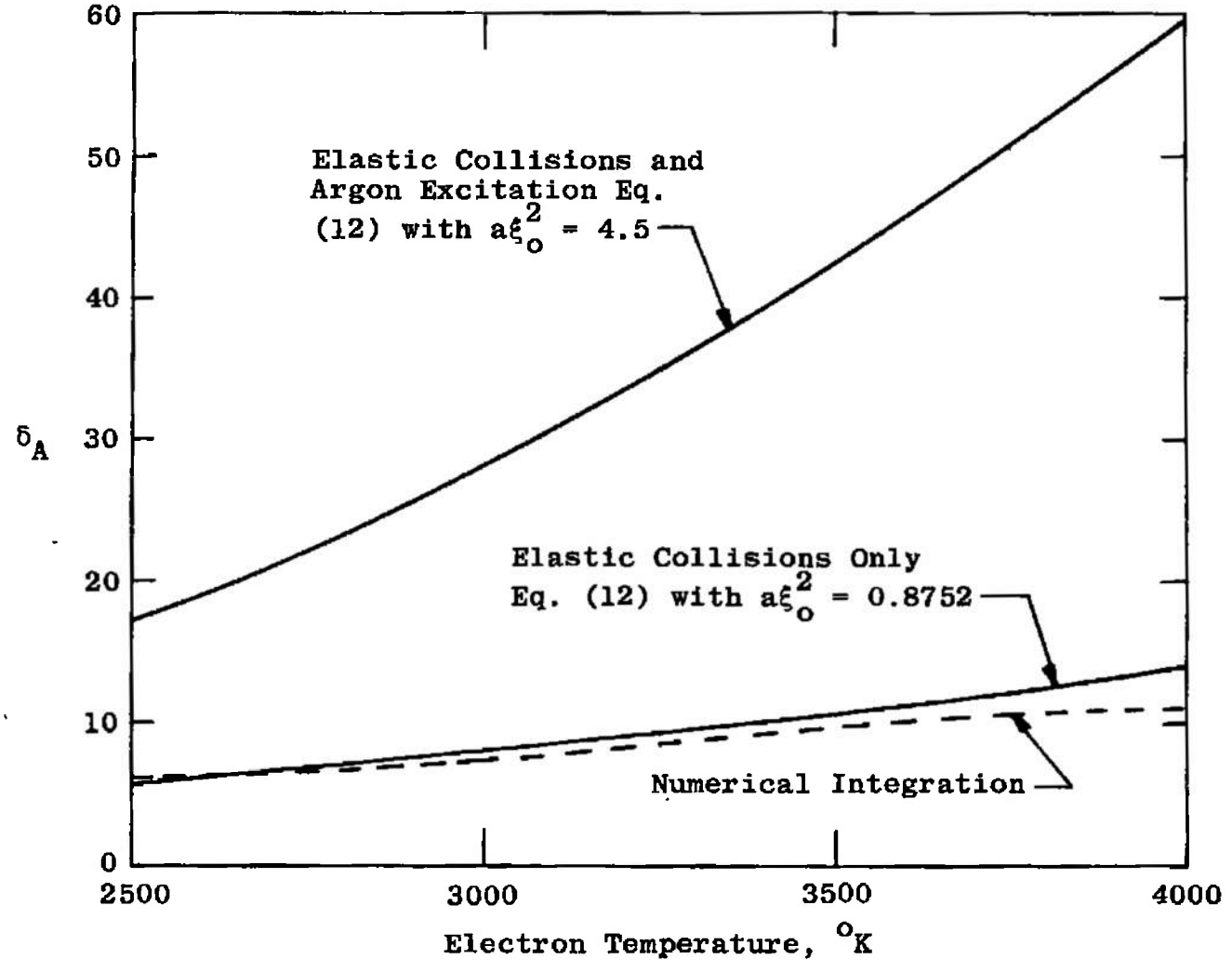

Fig. 4 Energy-Momentum-Loss Parameters for Argon

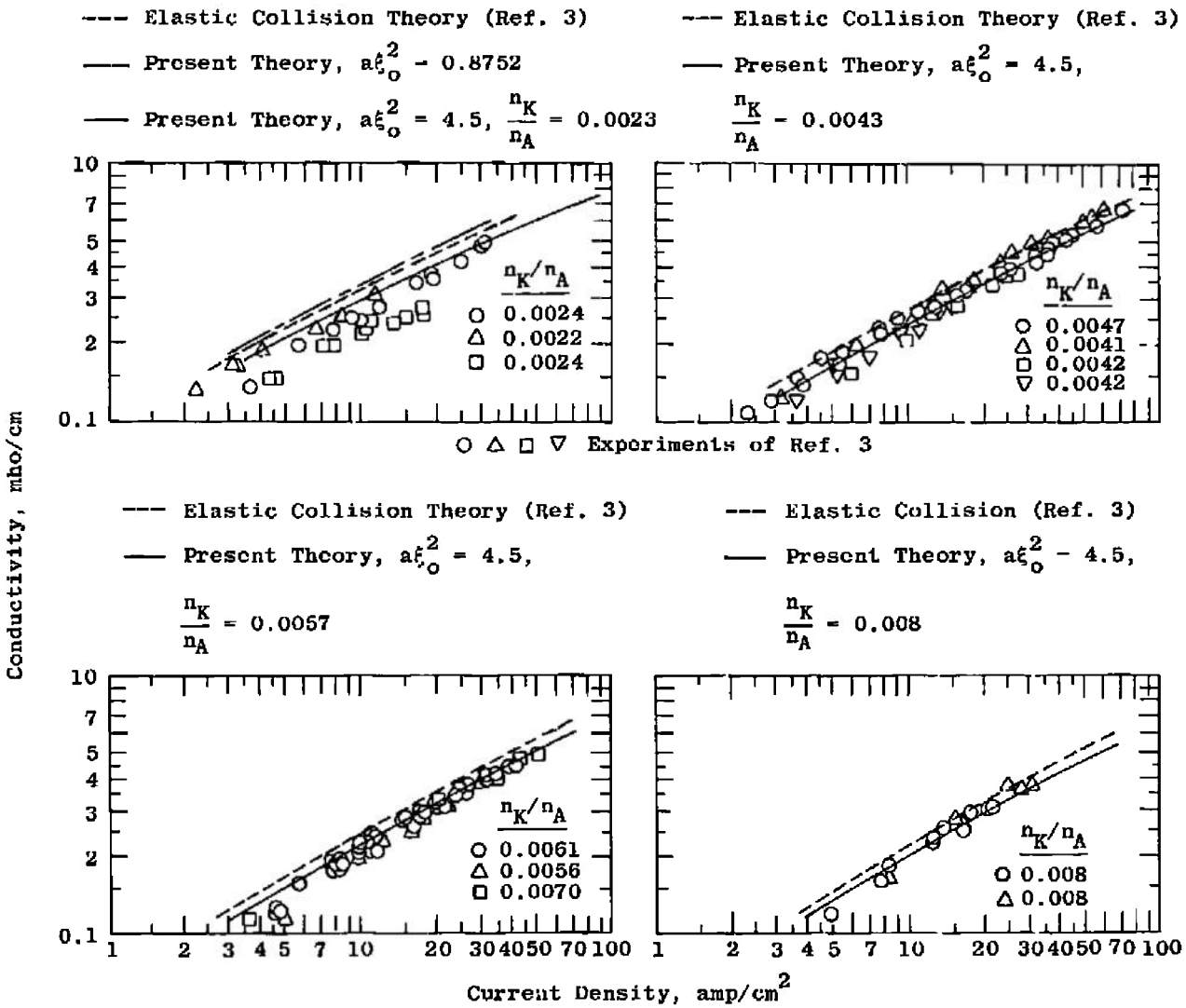

Fig. 5 Dependence of Steady-State Conductivity in Seeded Argon on Current Density, Seed Rate, and Electron-Energy Loss

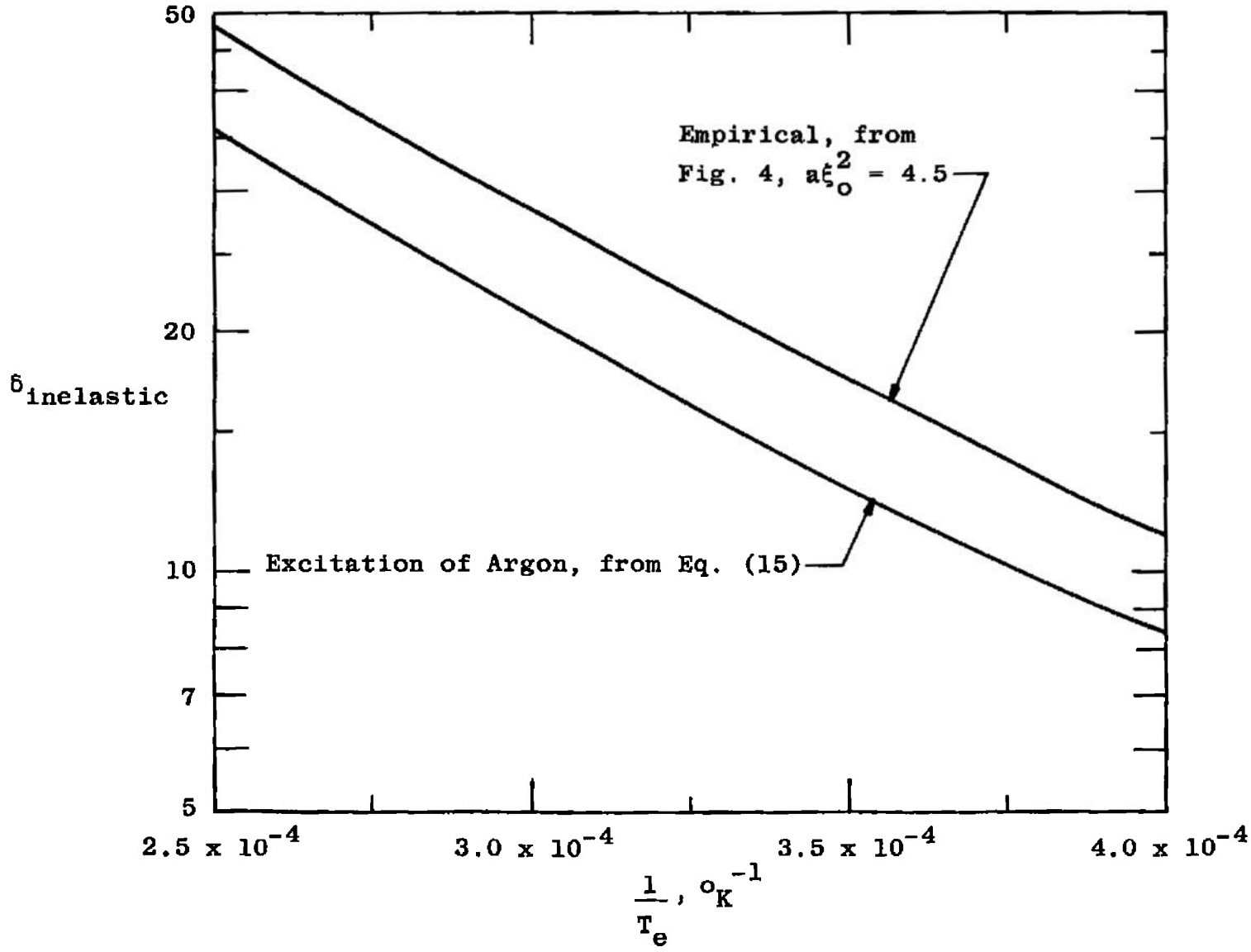

Fig. 6 Inelastic Collision Energy-Momentum-Loss Parameters for Argon

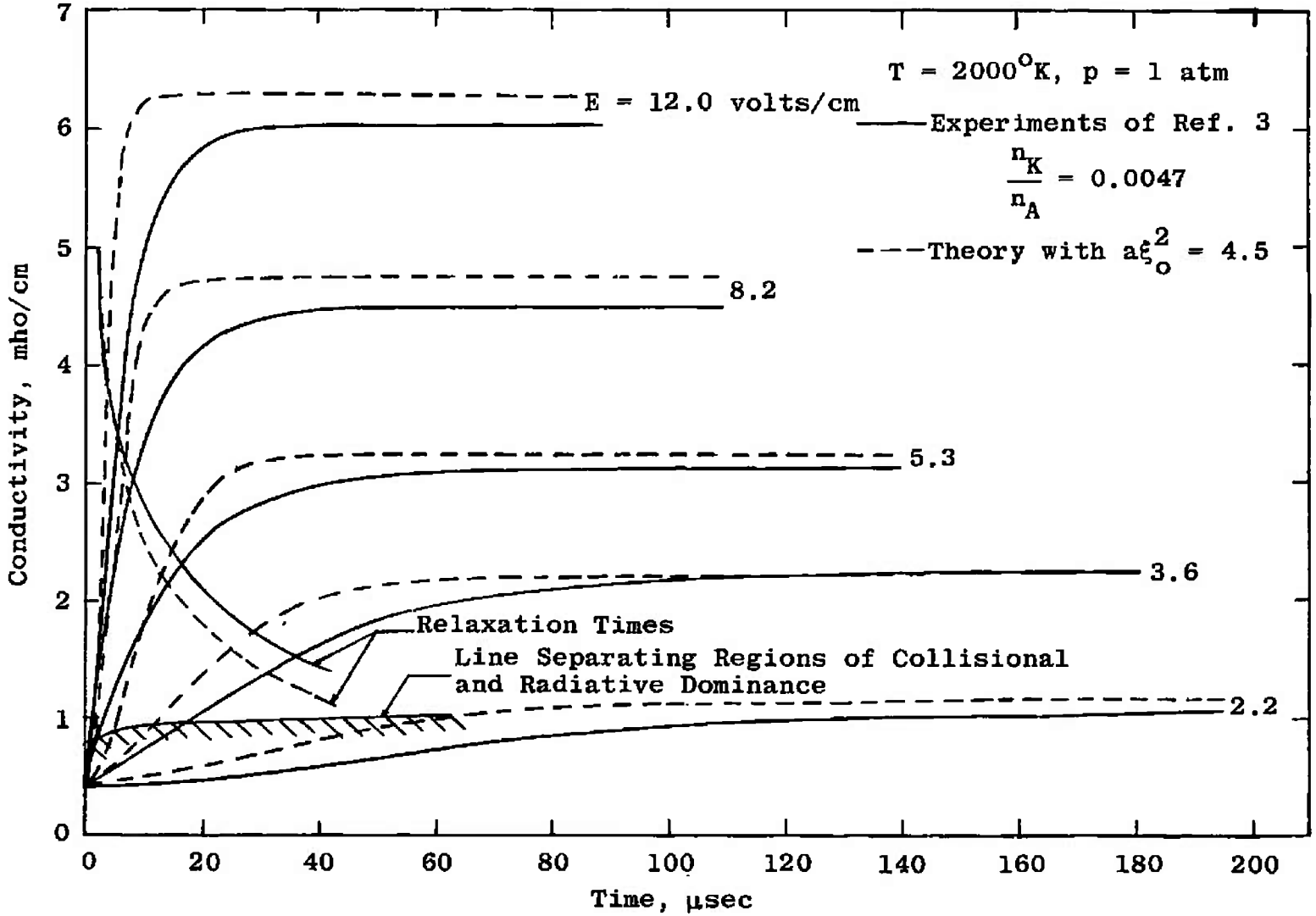

Fig. 7 Theoretical and Experimental Conductivity-Relaxation Profiles

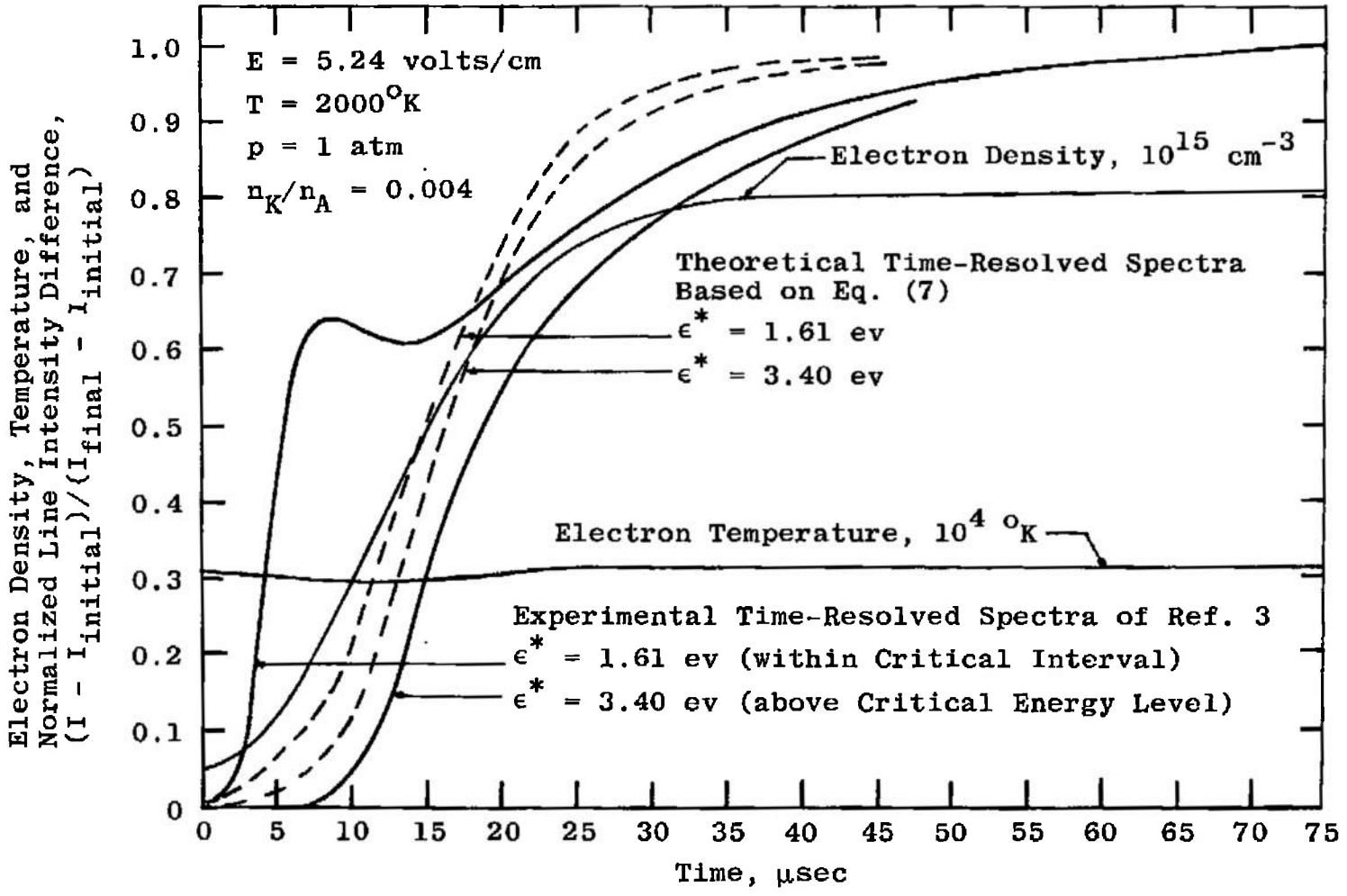

Fig. 8 Theoretical and Experimental Potassium Excited-State Relaxation Profiles

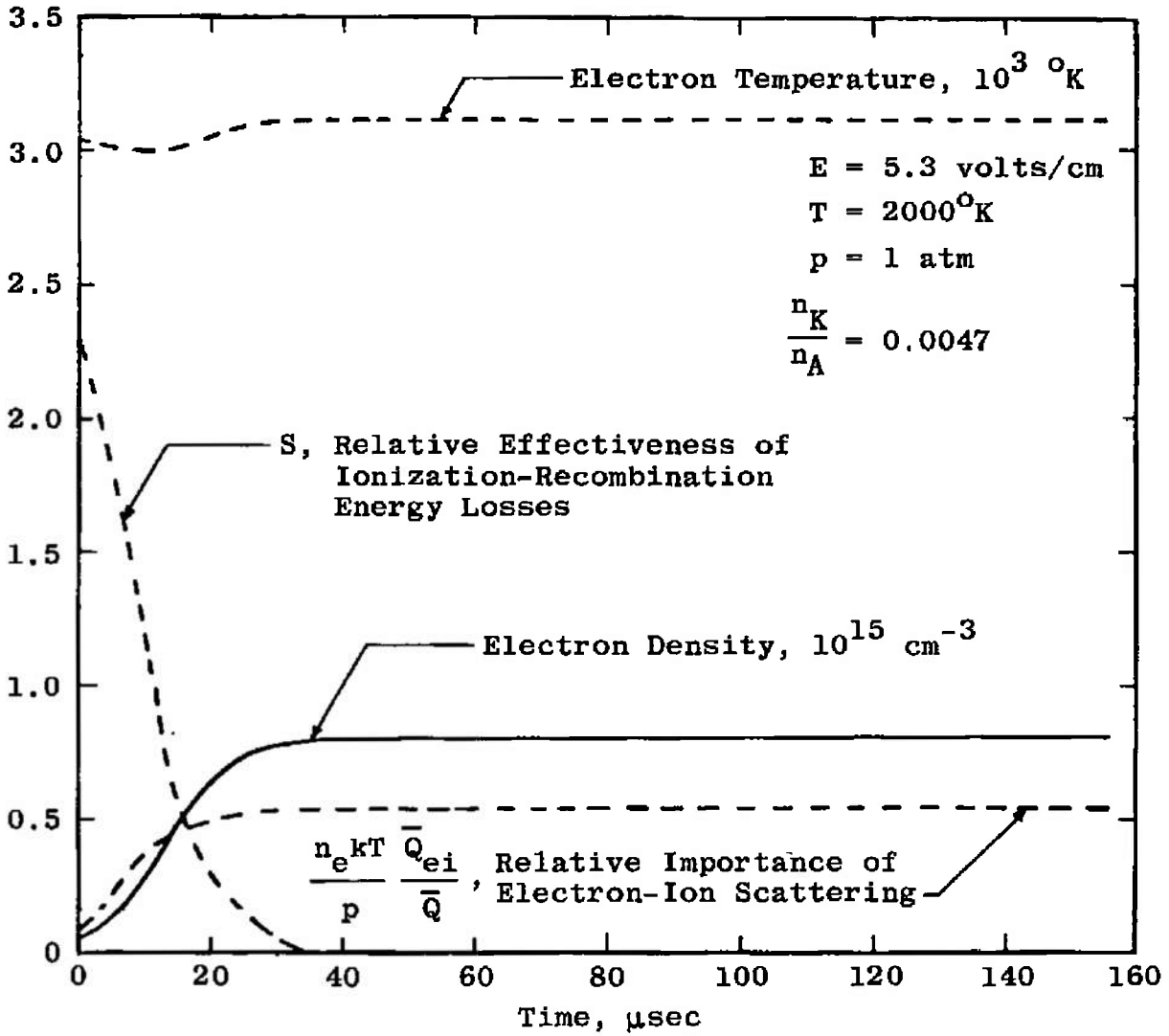

Fig. 9 Correlation of Relaxation Solutions with Collision Mechanisms

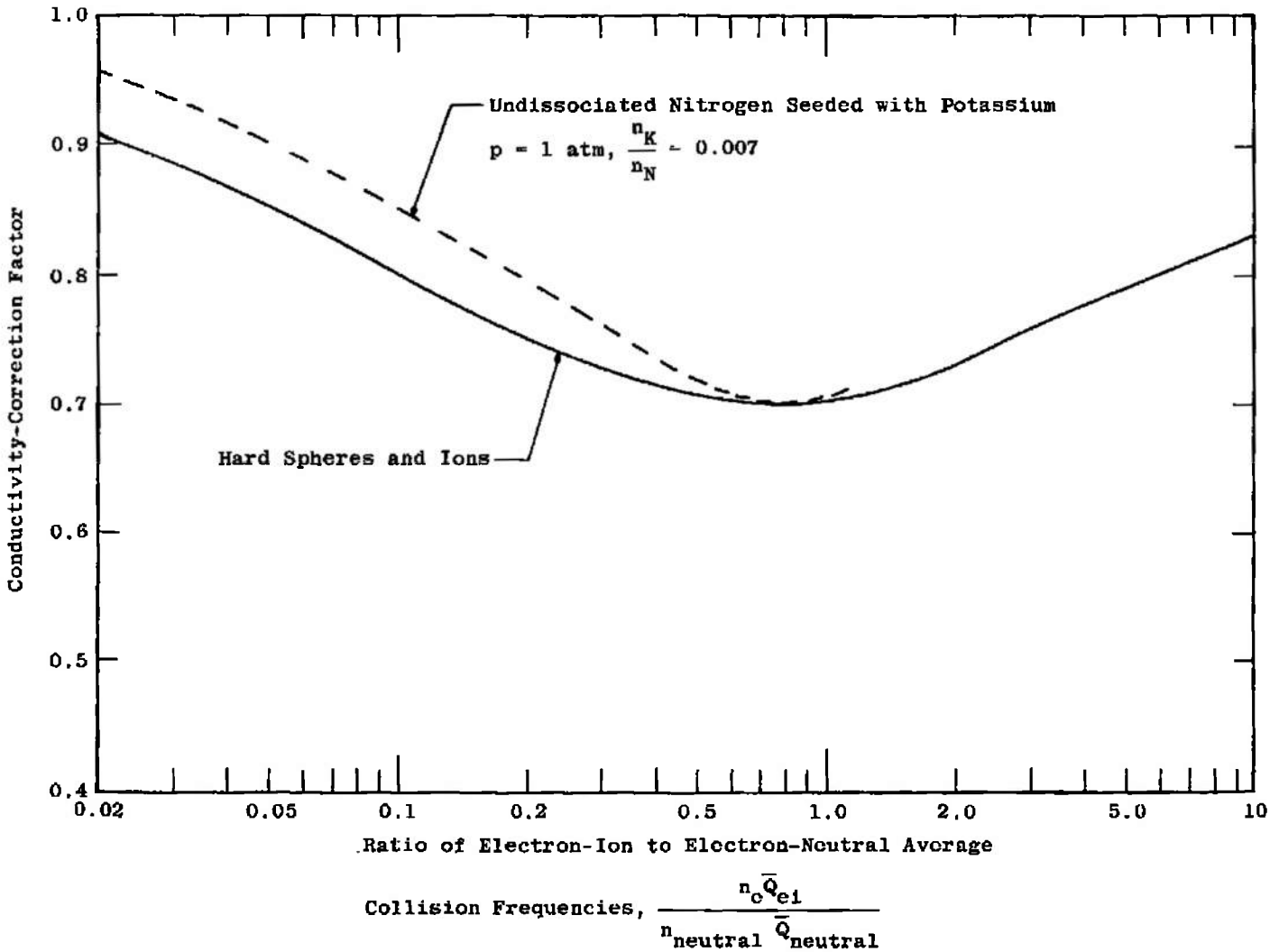

Fig. 10 Corrections to Conductivity According to Eq. (23), (H = 1)

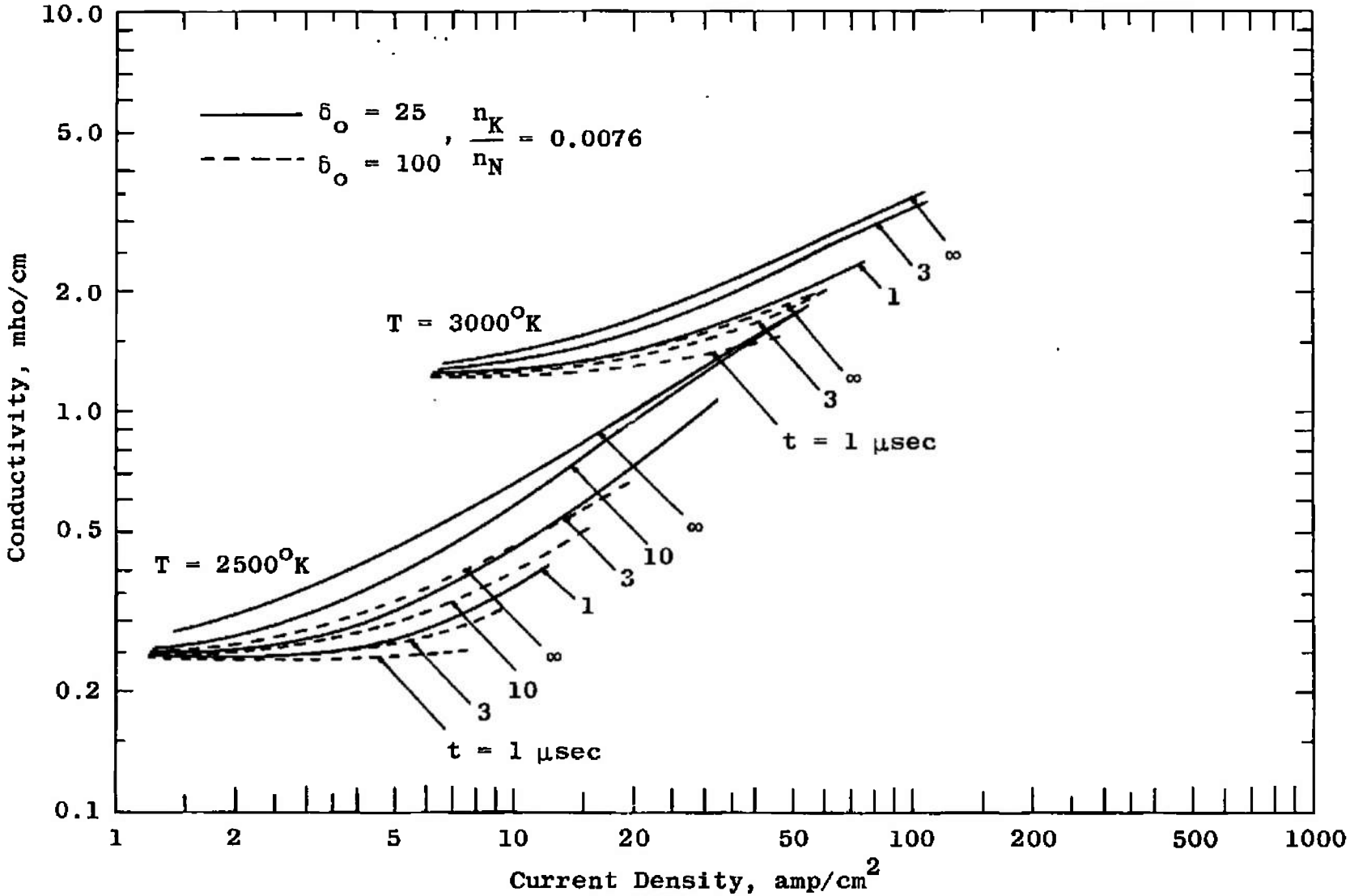

Fig. 11 Theoretical Dependence of Steady-State and Relaxing Conductivity in Seeded Nitrogen on Current Density, Temperature, and Electron-Energy Loss

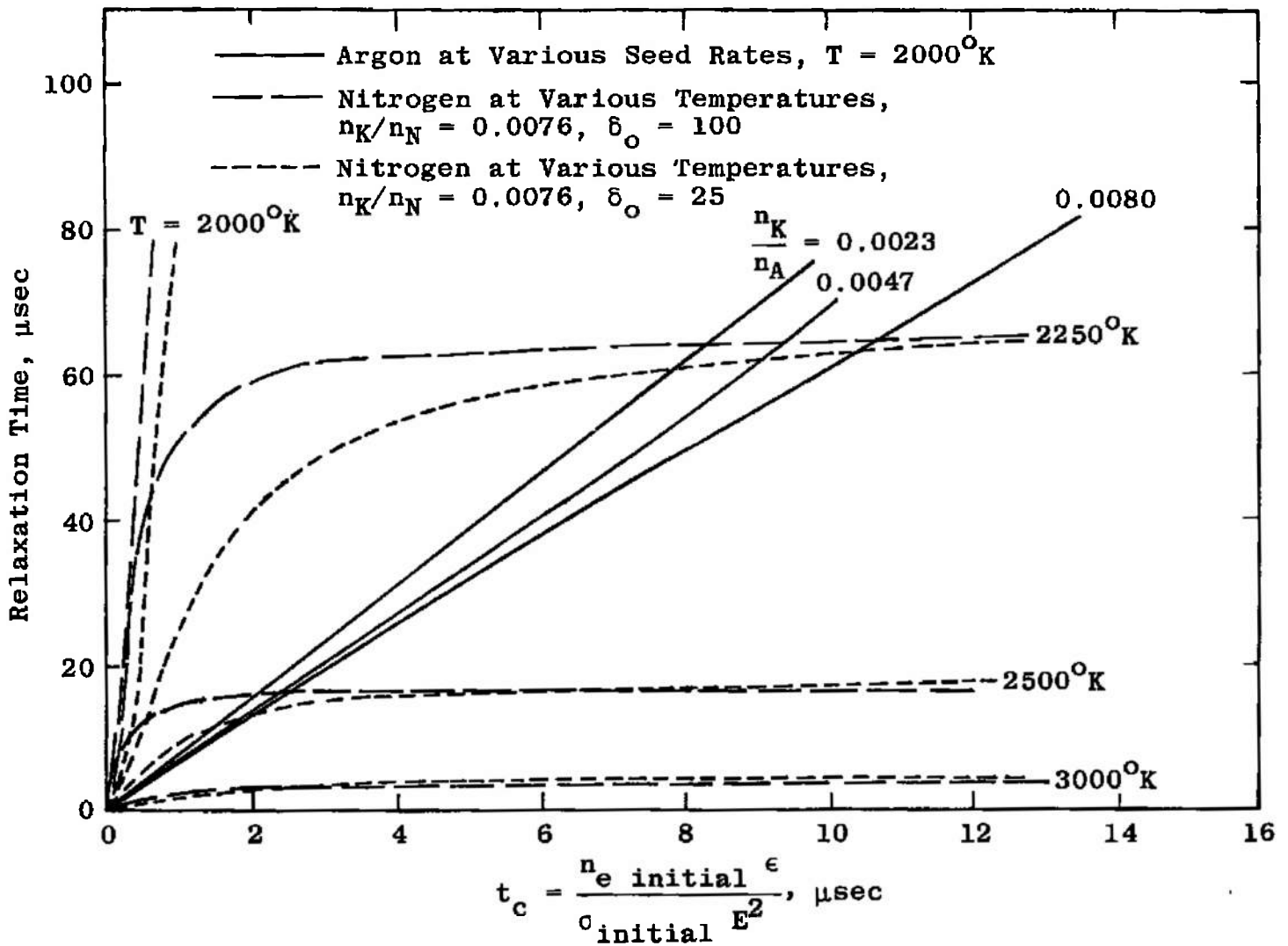

Fig. 12 Correlation of Relaxation Time with Characteristic Time Parameter for Power-Limited Relaxation

UNCLASSIFIED

Security Classification

DOCUMENT CONTROL DATA - R&D

(Security classification of title, body of abstract and indexing annotation must be entered when the overall report is classified)

1. ORIGINATING ACTIVITY (Corporate author)
Arnold Engineering Development Center
ARO, Inc., Operating Contractor
Arnold Air Force Station, Tennessee

2a. REPORT SECURITY CLASSIFICATION
UNCLASSIFIED

2b. GROUP
N/A

3. REPORT TITLE
RELAXATION TO THE STEADY STATE IN A CONDUCTING NONEQUILIBRIUM PLASMA STREAM

4. DESCRIPTIVE NOTES (Type of report and inclusive dates)
N/A

5. AUTHOR(S) (Last name, first name, initial)
Curry, Bill P., ARO, Inc.

6. REPORT DATE	7a. TOTAL NO. OF PAGES	7b. NO. OF REFS
April 1966	40	17

8a. CONTRACT OR GRANT NO.	9a. ORIGINATOR'S REPORT NUMBER(S)
AF 40(600)-1200 b. Program Element 65402234	AEDC-TR-66-43
c.	9b. OTHER REPORT NO(S) (Any other numbers that may be assigned this report)
d.	N/A

10. AVAILABILITY/LIMITATION NOTICES
Qualified users may obtain copies of this report from DDC and distribution of this document is unlimited.

11. SUPPLEMENTARY NOTES	12. SPONSORING MILITARY ACTIVITY
N/A	Arnold Engineering Development Center Air Force Systems Command Arnold Air Force Station, Tennessee

13. ABSTRACT

The relaxation of a seeded plasma subjected to a constant electric field is considered within the formalism of the two-temperature theory. Numerical solutions are obtained for streamwise conductivity profiles in both argon and nitrogen plasmas seeded with potassium. Reaction rates used here are analytical formulae based on the Byron model for collision-induced recombination. Extensive analysis of the computed results and comparison with Zukoski's experiments in argon establish the validity of the basic treatment and suggest the existence of energy losses resulting from excitation or argon transitions originating at the first excited state, in addition to the usual elastic collision and potassium excitation energy losses. Refined agreement between theory and experiment requires consideration of corrections to the species-averaged momentum-transfer cross section, after the manner of Frost; however, present theories are shown to overestimate this correction for argon. Details of the Byron model are validated by comparison of theoretical and experimental time-resolved potassium emission lines. Possible nonequilibrium effects in nitrogen are investigated with various assumed molecular excitation losses. Relaxation times for both types of plasmas are correlated by use of Zukoski's characteristic time parameter.

DD FORM 1 JAN 64 1473

UNCLASSIFIED

Security Classification

14. KEY WORDS	LINK A		LINK B		LINK C	
	ROLE	WT	ROLE	WT	ROLE	WT
plasmas						
potassium seeded						
relaxation						
nonequilibrium effects						
electric fields						
two-temperature theory						
energy losses						

INSTRUCTIONS

1. ORIGINATING ACTIVITY: Enter the name and address of the contractor, subcontractor, grantee, Department of Defense activity or other organization *(corporate author)* issuing the report.

2a. REPORT SECURITY CLASSIFICATION: Enter the overall security classification of the report. Indicate whether "Restricted Data" is included. Marking is to be in accordance with appropriate security regulations.

2b. GROUP: Automatic downgrading is specified in DoD Directive 5200.10 and Armed Forces Industrial Manual. Enter the group number. Also, when applicable, show that optional markings have been used for Group 3 and Group 4 as authorized.

3. REPORT TITLE: Enter the complete report title in all capital letters. Titles in all cases should be unclassified. If a meaningful title cannot be selected without classification, show title classification in all capitals in parenthesis immediately following the title.

4. DESCRIPTIVE NOTES: If appropriate, enter the type of report, e.g., interim, progress, summary, annual, or final. Give the inclusive dates when a specific reporting period is covered.

5. AUTHOR(S): Enter the name(s) of author(s) as shown on or in the report. Enter last name, first name, middle initial. If military, show rank and branch of service. The name of the principal author is an absolute minimum requirement.

6. REPORT DATE: Enter the date of the report as day, month, year; or month, year. If more than one date appears on the report, use date of publication.

7a. TOTAL NUMBER OF PAGES: The total page count should follow normal pagination procedures, i.e., enter the number of pages containing information.

7b. NUMBER OF REFERENCES: Enter the total number of references cited in the report.

8a. CONTRACT OR GRANT NUMBER: If appropriate, enter the applicable number of the contract or grant under which the report was written.

8b, 8c, & 8d. PROJECT NUMBER: Enter the appropriate military department identification, such as project number, subproject number, system numbers, task number, etc.

9a. ORIGINATOR'S REPORT NUMBER(S): Enter the official report number by which the document will be identified and controlled by the originating activity. This number must be unique to this report.

9b. OTHER REPORT NUMBER(S): If the report has been assigned any other report numbers *(either by the originator or by the sponsor)*, also enter this number(s).

10. AVAILABILITY/LIMITATION NOTICES: Enter any limitations on further dissemination of the report, other than those imposed by security classification, using standard statements such as:

(1) "Qualified requesters may obtain copies of this report from DDC."

(2) "Foreign announcement and dissemination of this report by DDC is not authorized."

(3) "U. S. Government agencies may obtain copies of this report directly from DDC. Other qualified DDC users shall request through _____."

(4) "U. S. military agencies may obtain copies of this report directly from DDC. Other qualified users shall request through _____."

(5) "All distribution of this report is controlled. Qualified DDC users shall request through _____."

If the report has been furnished to the Office of Technical Services, Department of Commerce, for sale to the public, indicate this fact and enter the price, if known.

11. SUPPLEMENTARY NOTES: Use for additional explanatory notes.

12. SPONSORING MILITARY ACTIVITY: Enter the name of the departmental project office or laboratory sponsoring *(paying for)* the research and development. Include address.

13. ABSTRACT: Enter an abstract giving a brief and factual summary of the document indicative of the report, even though it may also appear elsewhere in the body of the technical report. If additional space is required, a continuation sheet shall be attached.

It is highly desirable that the abstract of classified reports be unclassified. Each paragraph of the abstract shall end with an indication of the military security classification of the information in the paragraph, represented as *(TS)*, *(S)*, *(C)*, or *(U)*.

There is no limitation on the length of the abstract. However, the suggested length is from 150 to 225 words.

14. KEY WORDS: Key words are technically meaningful terms or short phrases that characterize a report and may be used as index entries for cataloging the report. Key words must be selected so that no security classification is required. Identifiers, such as equipment model designation, trade name, military project code name, geographic location, may be used as key words but will be followed by an indication of technical context. The assignment of links, rules, and weights is optional.